Empa
Materials Science and Technology

Characterization and modeling of orientation and size dependent tensile behavior of AM Ti6Al4V

Master Project

Daniele Ghedalia

August 16, 2019

Advisor: Dr. Ehsan Hosseini, EMPA Dübendorf

Department of Materials Science, ETH Zürich

Contents

Acknowledgments

First and foremost, I wish to acknowledge the help and guidance provided by my supervisor Ehsan Hosseini throughout the whole duration of this project. I would also like to thank Serjosha Robmann for his precious help and constant availability, and to the whole Experimental Continuum Mechanics Lab at Empa for the pleasant working environment.

Chapter 1

Introduction

Ti6Al4V is one of the most extensively researched and utilized titanium alloys, due to its overall superior properties. This alloy indeed exhibits high strength, low density, high fracture toughness, excellent corrosion resistance and biocompatibility [1]. Besides being widely employed in the aerospace sector, Ti6Al4V has found applications in the biomedical industry. The development of Ti6Al4V implants with customized porous architectures and mechanical properties is of particular interest, as their successful design and fabrication would enable the right conditions for bone ingrowth, adequate strength, and matched stiffness with respect to anatomical location [2].

To manufacture these kinds of structures, characterized by inherently complex geometries, the advanced manufacturing technology known as additive manufacturing (AM) is often required. Such technology enables the production of near-net shape components directly from CAD models by adding material in a layer-by-layer fashion. Several processes fall into this category, namely Direct Energy Deposition (DED), Electron Beam Melting (EBM) and Selective Laser Melting (SLM). The examined specimens of the present thesis were produced via SLM, a technique in which a focused laser beam scans the surface of a powder bed according to a prescribed path. The laser selectively melts the powders in each layer, after which a new layer of powders is spread after lowering the building platform to the distance of the layer thickness [3].

The foremost demand for Ti6Al4V is for load-bearing applications; this also holds for biomedical implants. The tensile and fatigue performances of AM Ti6Al4V lattice structures are key properties to consider for biomedical applications. It is hence of fundamental importance to fully characterize the influence of the numerous processing and material parameters on the final mechanical properties of AM Ti6Al4V lattice structures.

In this study, the effect of build orientation on the tensile properties of SLM Ti6Al4V struts constituent of lattice structures is investigated. Previous studies [4, 5] have already shown that due to the layer-wise nature of the SLM process, an anisotropic

microstructure in the printed samples is inevitably found. More specifically, the prior BCC-β grains grow in a columnar way almost parallel to the build direction through several layers in the range of 1-3 mm, while the average width of the prior β grains is in the order of 100 μm. When loaded, it has been shown that the dominant fracture mode happens along the prior-β grains. For these reasons, it is expected that the struts show different mechanical properties depending on the build orientation. The ultimate goal of this study is to develop an anisotropic material model that reliably describes the elastic-plastic tensile behavior of the Ti6Al4V struts. To achieve such a goal, an optimization-based approach is taken. The results of FEM simulations ran on the struts' true geometry (taken from X-ray Computer Tomography) are compared to the experimental results to derive a set of optimized material model parameters describing the deformation behavior.

Furthermore, this study examined struts with different nominal diameters (i.e. 200 to 500 μm). This is of particular interest because varying the struts' thickness enables a more tunable degree of porosity in lattice structures. Struts with diameters down to 200 μm are investigated: this range of thicknesses is smaller than what has previously been researched in literature. The existence of possible size effects that influence the struts' tensile properties will be studied. In this regard, no previous literature focusing on this aspect could be found.

Chapter 2

Material and Methods

2.1 Material

All the struts were manufactured at Renishaw plc., a British company that offers high-end systems and solutions for metal additive manufacturing. For their fabrication, an AM250 system, a laser power of 200 Watt, and Ti-6Al-4V powder were used. The powder was plasma-atomized to obtain a particle size of 14-45 μm. The layer thickness of the powder bed was 30μm. All specimens were annealed at 850 °C $\pm$ 10°C for 2 hours. No surface treatment and no hot isostatic pressing (HIP) treatment were performed. Table A.1 (see Appendix) provides some data about the powder composition of Ti-6Al-4V, as specified by the American Society for Testing and Materials (ASTM). Table A.2, instead, gives information about the mechanical properties of additively manufactured example components produced by Renishaw, using the Ti-6Al-4V powder and a layer thickness of 30μm.

The specimens were printed in four different directions (figure 2.1). The four different build orientations were 0° (horizontal struts), 30°, 60° and 90° (vertical struts), as illustrated in figure 2.1. The nominal struts' diameters were 200 μm, 300 μm, 400 μm, 500 μm.

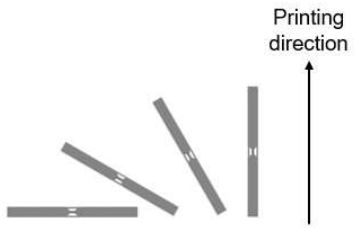

Figure 2.1: Schematic of struts printed with different orientations.

2.2 Mechanical testing

For all the struts, uni-axial tensile tests were performed in displacement-control mode at room temperature. A planar biaxial machine with horizontally mounted hydraulic actuators, and 100N load cells (MTS Systems, Eden Prairie, USA) was used to perform the tests. In a custom-built test setup, as shown in figure 2.2, the specimens were clamped at 9 mm from the distal end of the specimen between axes 1 and 3 of the machine. Axis 3 was used as the actuated one, while axis 1 was kept static. The imposed displacement rate was $2.5 * 10^{-4}$ mms^{-1}. A digital camera was positioned above the tested struts. Five pictures per second were taken during the test. The photos were then used in the post-processing phase, in order to measure the strain via Digital Image Correlation (DIC). The evaluation software GOM Correlate was used for this purpose.

In order to ensure statistical relevance for the results of the mechanical tests, at least six specimens for each strut family were tested, where with "strut family" a specific combination of build orientation and nominal diameter is meant. There are 16 of such strut families, as four build-orientation angles and four nominal strut diameters were considered.

In previous studies carried out in the Experimental Continuum Mechanics Laboratory at EMPA, a so called *compensation strategy* was adopted for the printing of the struts. This strategy proved to be successful for Bagheri et al. [2]. This was done as a measure against the significant *oversizing* of the struts' diameters compared to their nominal counterparts. This oversizing is particularly evident for horizontal and low build-orientation angle struts. In such struts, the laser beam melts multiple powder layers at once, causing previously melted layers to melt again. Furthermore, the reduced amount of heat dissipation for such struts compared to vertical ones causes heat localization.

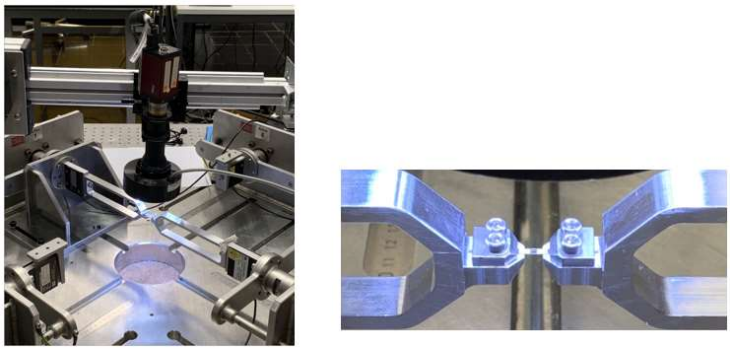

Figure 2.2: Experimental setup: MTS tensile testing machine (left) and close-up of a clamped strut specimen (right)

As shown in figure 2.3, this results in the fabrication of struts which are thicker than expected. As an example, the compensation strategy aimed at obtaining 200 μm used a nominal diameter of 100 μm in the CAD files used for printing horizontal samples. In this study, however, no compensation strategy was employed.

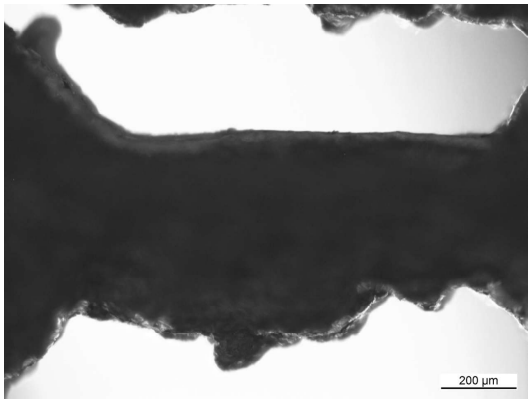

Figure 2.3: Light-microscope photo of a horizontal 300 μm strut

2.3 μCT and Light Microscopy

μCT was used to construct a digital model for the geometry of 3D printed samples. For the computerized-tomography of the specimens, a μCT machine with a nominal resolution of 5.6 μm was used. The 3D geometries of the specimens were then converted to a finite-element mesh using the software Materialise Mimics. The FE mesh was used for FE simulations replicating the mechanical testing procedure described in section 2.2. Further details are following in the next section.

To measure the struts' diameters, light microscopy photos were used: several measurements along the struts' length (typically 8 to 10 measurements) were taken to calculate the average diameter and the standard deviation for each strut. A 10x magnification was used to take photos such as the one shown in figure 2.3.

2.4 Finite Element Analysis and Optimization

In order to develop an anisotropic elastic-plastic material model for the Ti6Al4V struts, an optimization-driven approach was followed, in which the experimental force-strain curves for the CTed struts were combined with FE simulation results to develop a set of optimized material parameters.

2.4.1 Material Definition and Simulation Setup

The elastic response of the struts in the ABAQUS FE simulation was described by a transversely isotropic elasticity material model, in which only five constants are independent ($E_p, E_t, \nu_{pt}, \nu_{tp}, G_t$). The anisotropic yield properties were instead defined by the Hill's potential function, which is an extension of the Von Mises function [6]. An exponential function, derived from the Armstrong-Frederick law [7], was employed to describe the strain hardening response of the material.

3D models of the tested struts were created via computer tomography (CT) images using the software Materialise Mimics. These 3D models were then properly meshed using a tetrahedral C3D10 element type with an adaptive mesh size of 0.05 - 0.5 mm from surface to body. The meshed models of the struts were imported in ABAQUS, where local material coordinate systems in agreement with the printing orientations were set for each strut. Replicating the experimental procedure explained in section 2.2, the struts were subjected to a displacement ramp applied to one end of the strut, while the other end was fixed by the encastre boundary condition. The reaction forces were extracted and assumed to be representative of the force records from the testing machine.

2.4.2 Optimization

In order to derive the optimized material model parameters describing the anisotropic elastic-plastic behavior of the Ti6Al4V struts, a MATLAB script was written for this purpose. The script compares the experimental force-strain curves with the results of the FE simulations, and iteratively updates the model parameters to improve the consistency between the simulated and experimental force-strain responses. This approach is schematically illustrated by figure 2.4.

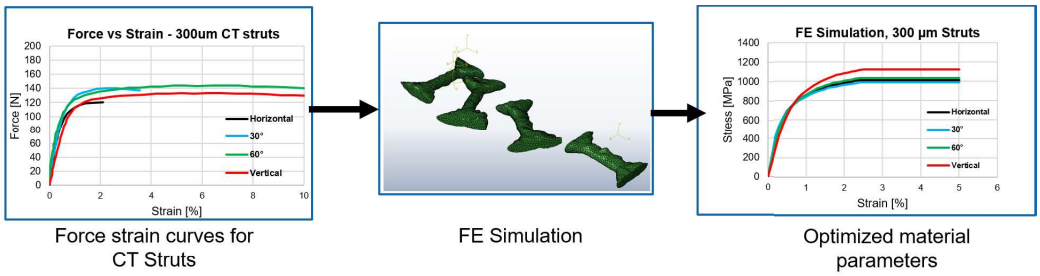

Figure 2.4: Schematic of the optimization-driven approach followed to obtain the optimized material mocel parameters

Chapter 3

Results

In this section, the experimental results of the tensile tests performed on the struts will be presented and discussed. First, the force-strain curves will be analyzed; then, the stress-strain curves will be discussed, with a specific focus on the effect of diameter measurement strategy on the obtained results. These results emphasize the need for an unbiased and accurate way of measuring the cross-sectional area of the struts. The section concludes with the results of the FE optimization.

3.1 Force-strain curves

The experimental force-strain curves for all strut families are displayed in figure 3.1. Six or seven struts were tested for each strut family. As expected, by increasing the nominal strut diameter, the force values at a given strain value raise significantly. In table 3.1 the mean force at 1% strain for all strut families are presented. This value was calculated by averaging over the force values at 1% strain for the 6 specimens belonging to each strut family. It can be seen that, for all orientations, the mean force value for the 500 μm struts is 4-5X higher than that for the 200 μm struts.

Mean force at 1% strain [N]				
	H	30	60	V
200um	51.00	61.97	54.33	51.98
300um	100.31	128.99	127.67	115.55
400um	137.67	189.55	161.20	176.02
500um	217.02	249.74	246.72	217.45

Table 3.1: The color legend shows that the mean force at 1% strain noticeably increases for increasing nominal diameter values

While these results are not surprising, it is more interesting to analyze what happens for struts of the same nominal diameter and different build-orientation angles (moving

horizontally across table 3.1). As highlighted by the color legend, the horizontal struts and the 30° struts appear to be the weakest and strongest, respectively. The overall trend for the mean force values is the following:

$$F_H < F_V < F_{60°} < F_{30°}$$

However, these results by themselves are not best suited to describe the anisotropic behavior of SLM Ti6Al4V: table 3.2 shows in fact that the 30° struts are actually the thickest ones for most strut diameters, whereas the vertical struts are in all cases the thinnest. The general trend for strut diameters (φ) is:

$$\varphi_V < \varphi_{60°} < \varphi_H < \varphi_{30°}$$

Table 3.3 describes the *oversizing* of the struts, which refers to how much bigger the struts diameters are relatively to their nominal value: $oversizing = \frac{average(\varphi)}{nominal(\varphi)}$. It can be observed that the oversizing considerably decreases with increasing nominal diameter values (moving downwards within the table) and increasing build-orientation angles (moving horizontally to the right across the table).

Mean diameter [um]				
	H	30°	60°	V
200 um	438.37	403.52	299.75	306.26
300 um	485.09	563.90	423.05	407.40
400 um	531.77	634.19	499.20	468.04
500 um	636.42	656.89	604.51	570.38

Table 3.2: Calculated mean diameters for all strut families. The legend describes increasing mean diameters for struts of the same nominal thickness.

Oversizing				
	H	30°	60°	V
200 um	2.19	2.02	1.50	1.53
300 um	1.62	1.88	1.41	1.36
400 um	1.33	1.59	1.25	1.17
500 um	1.27	1.31	1.21	1.14

Table 3.3: Oversizing of the average strut diameters with respect to the nominal values. The legend highlights a trend: thinner and lower build-orientation struts possess a higher degree of oversizing.

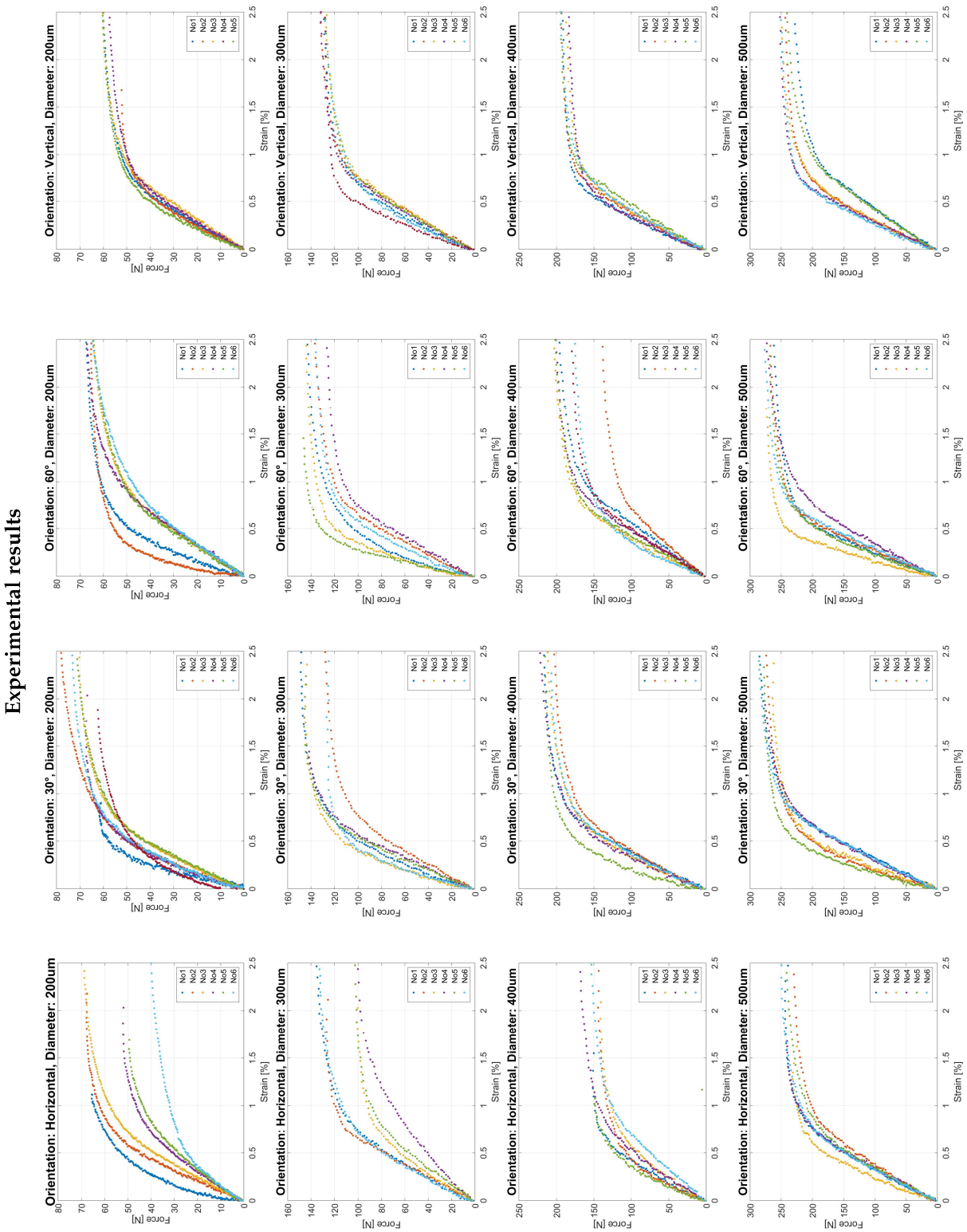
Experimental results
Orientation: Horizontal, Diameter: 200um
Orientation: 30°, Diameter: 200um
Orientation: 60°, Diameter: 200um
Orientation: Vertical, Diameter: 200um
Orientation: Horizontal, Diameter: 300um
Orientation: 30°, Diameter: 300um
Orientation: 60°, Diameter: 300um
Orientation: Vertical, Diameter: 300um
Orientation: Horizontal, Diameter: 400um
Orientation: 30°, Diameter: 400um
Orientation: 60°, Diameter: 400um
Orientation: Vertical, Diameter: 400um
Orientation: Horizontal, Diameter: 500um
Orientation: 30°, Diameter: 500um
Orientation: 60°, Diameter: 500um
Orientation: Vertical, Diameter: 500um
Force [N]
Strain [%]
No1
No2
No3
No4
No5
No6

3.2 Stress-Strain curves

In order to precisely assess the build-orientation-dependent tensile behavior of the struts, it is then necessary to represent the observations in the form of stress-strain curves rather than force-strain curves. This naturally entails measuring the cross-sectional area for each strut, by which the force values will then be normalized in order to determine the stresses. This seemingly simple task unfortunately involves a certain degree of arbitrariness, as shown by figure 3.1. In fact, the lower orientation struts (horizontal and 30°) are not only the most oversized, but also display the most pronounced waviness and irregularities along their length.
In this regard, table 3.4 describes the coefficient of variation (which we can interpret as waviness) in each strut family. This value was calculated in the following way: the standard deviation of each strut's diameter was calculated, by taking 6-7 measurements along its length using images taken at the light microscope. This procedure was performed for each of the 6-8 samples belonging to each strut family, and the average value was calculated. Finally, this number was divided by the strut family's average diameter and multiplied by 100 to obtain a percentage value: $Waviness = \frac{Avg[St.Dev.(\varphi_{singlestrut})]}{Avg(\varphi_{singlestrut})} * 100$

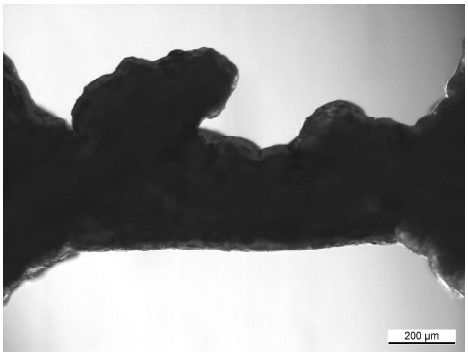

Figure 3.1: Optical microscopy image showing a 200 μm strut with horizontal orientation

Waviness [%]				
	H	30°	60°	V
200 um	19.77	11.71	4.12	6.38
300 um	10.54	11.91	3.74	3.40
400 um	12.80	6.03	3.54	3.44
500 um	7.99	5.10	4.58	4.28

Table 3.4: Waviness for all strut families. The legend highlights increased waviness for thinner and lower build-orientation angle struts.

The results from table 3.4 clearly show that the horizontal and 30° struts exhibit a higher level of waviness compared to the other two strut families. At the same time, it appears that thicker struts display a decreased amount of waviness.

Two different approaches were then employed and compared in order to determine the stresses: considering the average and minimum diameters. The following plots show the experimental stress-strain curves taken for the samples which had been scanned by computer tomography, which from now will be termed "CT struts". The CT struts were considered as being representative for each strut family: it was in fact checked that their force-strain curves fall within the lower and higher boundary curves of their respective strut families.

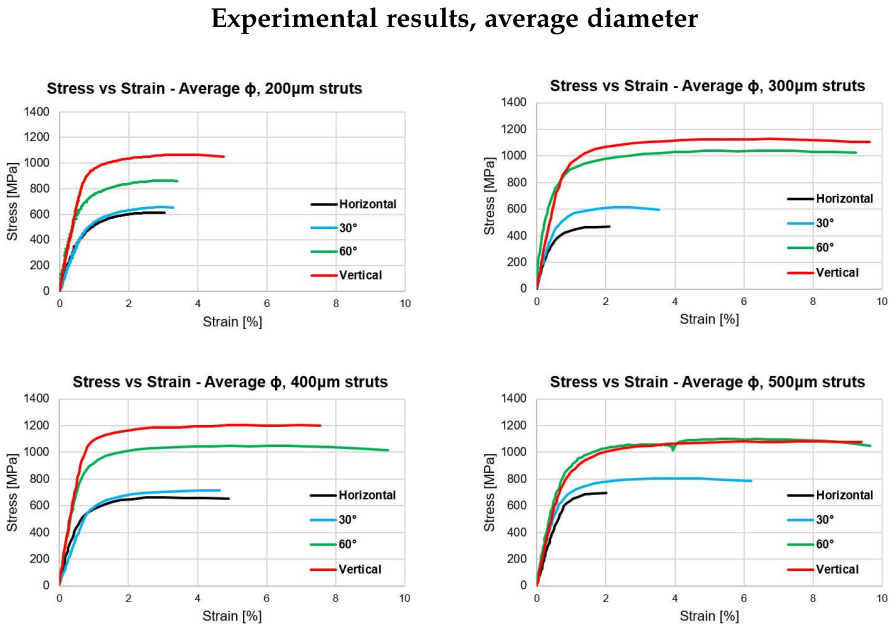

Figure 3.2: Stress-strain curves for the CT struts, calculated by using the measured average diameter

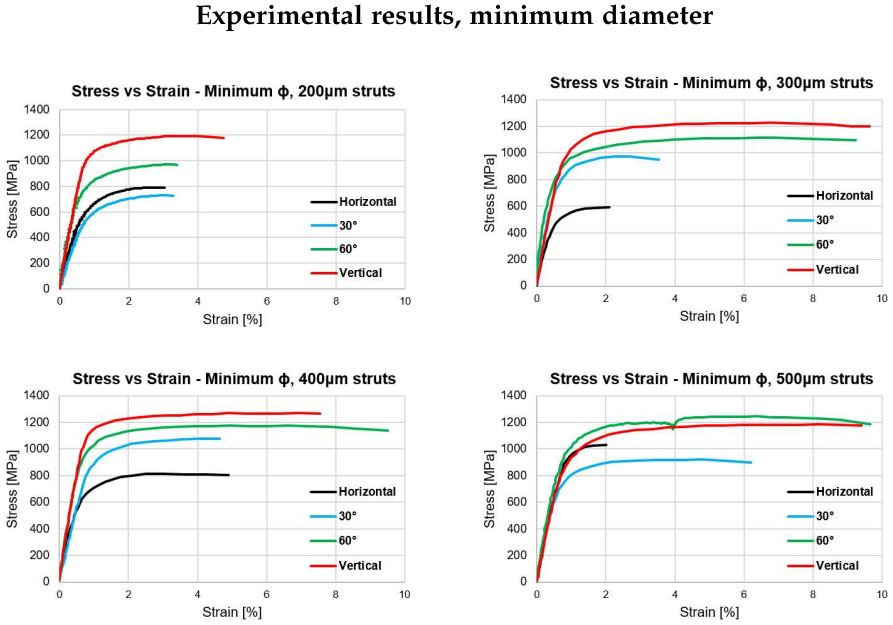

Figure 3.3: Stress-strain curves for the CT struts, calculated by using the measured minimum diameter

With regards to the plots shown above, some observations can be made. The vertical struts are the strongest, and the horizontal ones are the weakest. Simultaneously, increasing the build-orientation angle positively correlates with ductility, as the 60° and vertical struts have much higher strains at failure. However, the gap in stress values between the high build-orientation angle struts (vertical and 60°) and the low build-orientation angle struts (horizontal and 30°) is unexpectedly high. This might be explained by the procedure which was used to measure the struts' diameters.

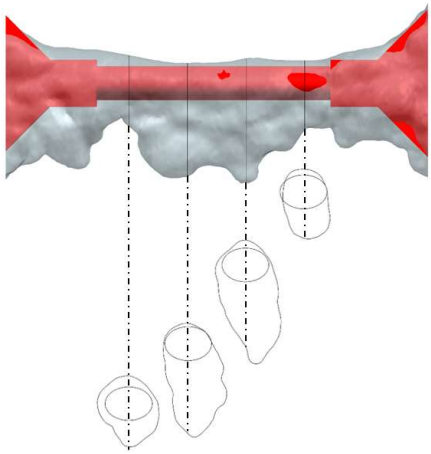

Figure 3.4: Cross-sections of a highly irregular strut as observed from computer-tomography photos. It is clear that the 2D view offered by the light microscope photos is highly restrictive for the sake of precise cross-sectional area determination. Courtesy of Serjosha Robmann.

Light microscope pictures like the one showed in figure 3.1 were used for this purpose. CT data have shown that unlike vertical struts, horizontal and 30° struts display highly irregular and non-circular cross-sectional shapes, as shown in figure 3.4. This probably causes the diameters of such struts to be significantly overestimated when measured at the light microscope. In support of this claim, it can be observed that when switching from average to minimum diameters, the stress-strain curves for the horizontal and 30° struts undergo a non-negligible shift towards higher stresses, whereas this effect is much more moderate for the 60° and vertical struts. Indeed, the previously mentioned unrealistically high gap between the high and low build-orientation angle struts decreases when using the minimum diameter to calculate the cross-sectional area of the struts.

These findings highlight the need for a more accurate way of measuring the struts' cross-sectional areas, in order to derive reliable stress-strain curves that precisely describe the material's deformation behavior as a function of the printing orientation.

3.3 Investigation on possible size effect

To determine whether the strut diameter has any effect on its deformation response. stress-strain curves for struts of the same build orientation but different diameters were plotted, as shown in figure 3.5

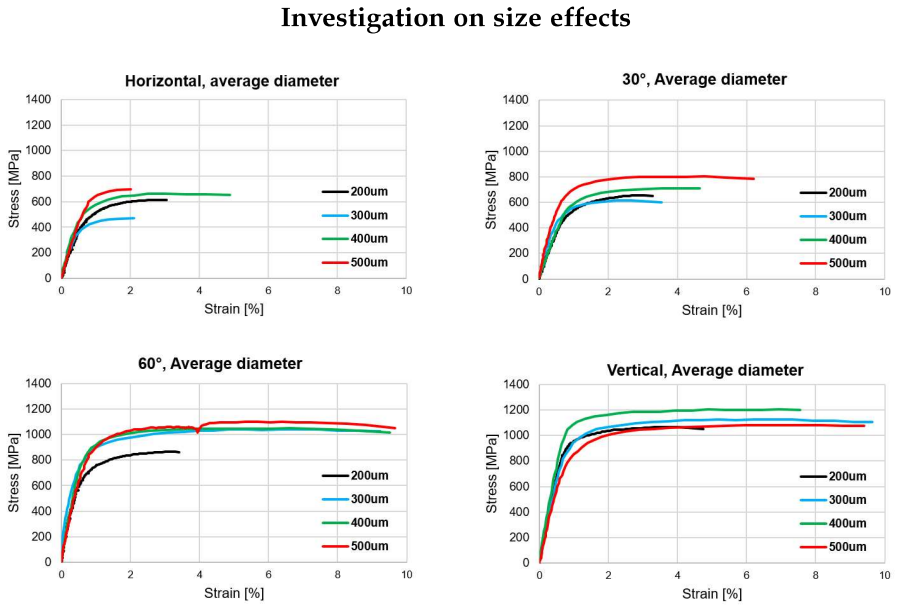

Figure 3.5: Comparison of stress-strain curves for struts with the same orientation but different diameters. Average diameters were used for calculation of stress.

For such curves, the average diameter was used to calculate the stress values. It can be noticed that no clear trend with regard to size-dependency appears to exist. However, as highlighted at the end of section 3.2, diameter measurements taken from the 2D view offered by the microscope photos might lead to inaccurate or deceiving results. To confidently confirm that no size effects exist, employment of FE analysis is a more appropriate method.

3.4 Finite Element Analysis and Optimization results

In order to address the problem of the struts' cross-sectional area measurements and their effects on the calculated stress-strain curves, the FE optimization-driven approach described in section 2.4.1 and 2.4.2 was undertaken. Figure 3.6 shows derived stress-strain curves from the FE optimization for the 300 μm struts.

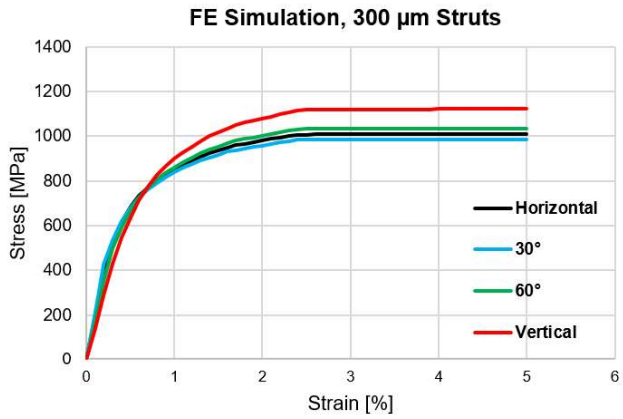

Figure 3.6: Optimized stress-strain curves for 300 μm struts with different build orientations

These results confirm that the vertical struts are the strongest, with an ultimate tensile stress of about 1100 MPa. At the same time, the other orientations exhibit higher strength levels compared to the experimental results (i.e. figures 3.2 and 3.3). Also, the gap in strength between the vertical struts and the other strut families is now greatly reduced, similarly to what we would expect. At the time of writing, FE-based optimization for other strut diameters is still ongoing.

Chapter 4

Conclusion and Outlook

It has been observed that the printed struts exhibit large geometrical mismatches relatively to their nominal geometries. The struts exhibit considerable oversizing, especially for smaller nominal diameters and lower build-orientation angles. Additionally, considerable waviness has been observed, notably for lower build-orientation struts. Two approaches have been taken in order to calculate the stress-strain curves, namely to choose the average and minimum diameters in order to calculate the struts' cross-sectional areas. These two approaches resulted in non-negligible different stress values, especially for horizontal and 30° struts, highlighting the difficulty and arbitrariness inherent to measuring the struts' diameters.

These considerations highlighted the need for a more consistent and reliable method to assess the orientation-dependent deformation behavior of the struts, suggesting a FE optimization-driven approach that utilizes the struts' real geometries taken via micro-computerized tomography.

Due to the limited time of this semester project and to the long duration of the FE optimization, only preliminary results are available at the time of writing. Results for the 300 μm struts showed that the vertical struts are the strongest and that the horizontal are the weakest.

Ideally, a correlation factor between the cross-sectional area measured in the microscope photos and the true area as observed in the CT geometry could be derived for different build-orientation angles, in order to avoid the lengthy and expensive procedure inherent to μCT scanning and FE optimization.

Additionally, further effort can be spent in order to extend the optimization so that both the orientation and the diameters can be jointly considered, in order to develop an anisotropic material model.

Appendix A

Appendix

Element	Mass (%)
Titanium	Balance
Aluminium	5.50 to 6.50
Vanadium	3.50 to 4.50
Iron	≤ 0.25
Oxygen	≤ 0.13
Carbon	≤ 0.08
Nitrogen	≤ 0.05
Hydrogen	≤ 0.012
Yttrium	≤ 0.005
Residuals	≤ 0.10 each, ≤ 0.40 total

Table A.1: Composition of Ti-6Al-4V powder as specified by the ASTM

	Heat treated (See note 2)		**HIP treated** (see note 6)	
	Mean	**Standard deviation (±1σ)**	**Mean**	**Standard deviation (±1σ)**
Ultimate tensile strength (UTS) (See note 3)				
Horizontal direction (XY)	1089 MPa	7 MPa	1033 MPa	4 MPa
Vertical direction (Z)	1085 MPa	12 MPa	1034 MPa	7 MPa
Yield strength (see note 3)				
Horizontal direction (XY)	1007 MPa	5 MPa	947 MPa	4 MPa
Vertical direction (Z)	985 MPa	23 MPa	923 MPa	21 MPa
Elongation at break (See note 3)				
Horizontal direction (XY)	16%	1%	16%	1%
Vertical direction (Z)	14%	1%	17%	1%
Modulus of elasticity (see note 3)				
Horizontal direction (XY)	129 GPa	7 GPa	127 GPa	3 GPa
Vertical direction (Z)	126 GPa	15 GPa	125 GPa	4 GPa
Hardness (Vickers) (see note 4)				
Horizontal direction (XY)	368 HV0.5	10 HV0.5	352 HV0.5	9 HV0.5
Vertical direction (Z)	372 HV0.5	7 HV0.5	360 HV0.5	7 HV0.5
Surface roughness (R_a) (See note 5)				
Horizontal direction (XY)	4 µm to 6 µm			
Vertical direction (Z)	4 µm to 7 µm			

Table A.2: Mechanical properties of exemplary AM Ti-6Al-4V parts produced by Renishaw with a layer thickness of 30mm

List of Figures

List of Tables

Bibliography

[1] Matthew J Donachie. Titanium. *A Technical Guide, ASM International, Materials Park, OH*, 2000.

[2] Zahra S Bagheri, David Melancon, Lu Liu, R Burnett Johnston, and Damiano Pasini. Compensation strategy to reduce geometry and mechanics mismatches in porous biomaterials built with selective laser melting. *Journal of the mechanical behavior of biomedical materials*, 70:17–27, 2017.

[3] Chor Yen Yap, Chee Kai Chua, Zhi Li Dong, Zhong Hong Liu, Dan Qing Zhang, Loong Ee Loh, and Swee Leong Sing. Review of selective laser melting: Materials and applications. *Applied physics reviews*, 2(4):041101, 2015.

[4] Jingjing Yang, Hanchen Yu, Zemin Wang, and Xiaoyan Zeng. Effect of crystallographic orientation on mechanical anisotropy of selective laser melted ti-6al-4v alloy. *Materials Characterization*, 127:137–145, 2017.

[5] Marco Simonelli, Yau Yau Tse, and Christopher Tuck. Effect of the build orientation on the mechanical properties and fracture modes of slm ti–6al–4v. *Materials Science and Engineering: A*, 616:1–11, 2014.

[6] Michael Smith. *ABAQUS/Standard User's Manual, Version 6.9*. Simulia, 2009.

[7] Yanyao Jiang and Peter Kurath. Characteristics of the armstrong-frederick type plasticity models. *International Journal of Plasticity*, 12(3):387–415, 1996.

ETH

Eidgenössische Technische Hochschule Zürich
Swiss Federal Institute of Technology Zurich

Declaration of originality

The signed declaration of originality is a component of every semester paper, Bachelor's thesis, Master's thesis and any other degree paper undertaken during the course of studies, including the respective electronic versions.

Lecturers may also require a declaration of originality for other written papers compiled for their courses.

I hereby confirm that I am the sole author of the written work here enclosed and that I have compiled it in my own words. Parts excepted are corrections of form and content by the supervisor.

Title of work (in block letters):

CHARACTERIZATION AND MODELING OF ORIENTATION AND SIZE DEPENDENT BEHAVIOR OF AM TI6AL4V

Authored by (in block letters):

For papers written by groups the names of all authors are required.

Name(s):	**First name(s):**
GHEDALIA	DANIELE

With my signature I confirm that

- I have committed none of the forms of plagiarism described in the ' ' information sheet.
- I have documented all methods, data and processes truthfully.
- I have not manipulated any data.
- I have mentioned all persons who were significant facilitators of the work.

I am aware that the work may be screened electronically for plagiarism.

Place, date	**Signature(s)**
ZURICH, 21/08/2019	

For papers written by groups the names of all authors are required. Their signatures collectively guarantee the entire content of the written paper.